JOURNAL OF MATERIALS SCIENCE **38** (2003) 351 – 362

Effect of microstructure on properties of ADI and low alloyed ductile iron

A. REFAEY
Mechanical Engineer, Geisum Oil Company, No. 10, 250 st. Sarayat, Maadi, P.O. Box. 282, Cairo, Egypt

N. FATAHALLA
Professor of Materials Science, Mechanical Department, Faculty of Engineering, Al Azhar University, 11371 Nasr City, Cairo, Egypt
E-mail: nfatahalla@frcu.eun.eg

Microstructure, tensile, impact, hardness, fractography and wear characteristics were investigated for: (1) Austempered ductile iron (ADI); and (2) low alloyed ductile iron. Comparison has been made between the properties of these two types and that of conventional ductile iron. Detailed analysis, of the fracture mode for the 3 types of ductile iron, which failed under tensile and impact testing, were presented using the SEM. The wear properties were determined using pin-on-ring machine, under dry sliding conditions. The variation of mass loss and coefficient of friction with sliding distance, at different loads and speeds were presented and discussed. The wear mechanisms were investigated by means of subsurface observations. Microhardness test was used to study the change in the matrix strength with distance from the worn surface due to plastic deformation.
© *2003 Kluwer Academic Publishers*

1. Introduction

Ductile iron (DI) have significantly good combination of tensile strength, ductility and toughness, along with good wear resistance, and hardenability [1]. The recent development is to obtain a variety of bainitic structures [2]. Bainitic matrix in DI can be obtained in two ways: (i) In the as-cast form where bainitic transformation is achieved by judicious alloying elements such as Ni, Mo and Cr, (ii) By subjecting conventional DI castings to a specific heat treatment known as austempering [2]. ADI is present now as an attractive alternative to steel [3]. It shows high toughness, excellent wear resistance, and cost less than that of steel casting. Because of their superior properties and low production cost, ADIs have been increasingly used for industrial parts such as gears, crankshafts and cylinder heads [3]. The main objective of the present research is to investigate the relationship between microstructure, from one side, mechanical properties, fracture phenomena and wear characteristics of ADI and low alloyed DI from the other side compared with the conventional DI. Additionally, the research aimed at producing ADI having mechanical and wear properties comparable to those of low alloyed DI.

2. Experimental procedures

2.1. Materials, melting and casting

Conventional DI was produced using a high frequency induction furnace. The charge was made up of 80% pig iron with 3.9% C (all percentage are in mass%), 0.9% Si, and 20% ductile iron return, with 3.6% C, 2.4% Si and 0.05% Mg. The liquid metal was then treated (1.6% by weight of charge) with Fe-Si-Mg alloy (45, 50 and 5% respectively). The melt was then inoculated (0.6% by weight of charge), using Fe-Si alloy (20 and 80% by weight, respectively), having a grain size of 0.2–3 mm. The Sandwich technique [4] was used in producing DI iron. On the other hand, addition of the following master alloys produced the low alloyed DI: $FeNi_{95,}$ $FeMo_{70,}$ $FeMn_{70,}$ and $FeCr_{70,}$ in the as cast condition. Table I shows the chemical analysis of conventional DI before and after Mg-treatment and low alloyed DI. To maintain the same solidification cooling rate (SCR) and other casting conditions, the melts were poured into sand moulds with dimensions of ($120 \times 100 \times 75$ mm^3).

2.2. Tempering and austempering

Tempering was carried out for the low alloyed DI block at 873 K for 7.2 ks in a heating furnace. On the other hand, the austempering process details are shown in Fig. 1.

2.3. Metallography

Standard metallographic techniques [5] were employed to reveal the different micro-constituents of the structure. Optical microscopy was performed on polished and 2% nital etched specimens. The SEM used has a maximum magnification of about 10,000×.

2.4. Tension, impact and hardness tests

Static tension test was carried out according to ASTM specification E8, with a cross-head speed of

TABLE I Chemical analysis of the conventional DI before and after magnesium treatment and low alloyed DI

Condition	Element									
	C	Si	S	Mn	P	Mg	Cr	Ni	Mo	%C.E.
Before Mg treatment	3.75	1.30	0.010	0.75	0.040	0.003	0.06	0.02	—	4.33
After Mg treatment	3.45	2.43	0.009	0.089	0.042	0.06	0.061	0.024	—	4.60
Low alloyed	3.53	1.42	0.006	0.60	0.037	0.045	0.750	2.20	0.52	4.18

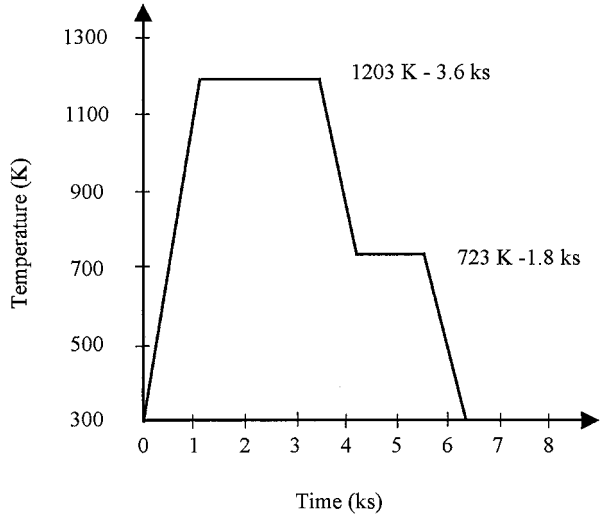

Figure 1 Schematic drawing of heat treatment cycle used in the present investigation.

2.7×10^{-2} mm/s and strain rate equal to 15×10^{-4} s^{-1}. Charpy V-notched and unnotched bar impact tests were machined according to ASTM-E23-1990. The maximum energy of the machine was 215 J, and impact velocity of 4.4 m/s. Macrohardness tests were performed using three indentation hardness methods. Microhardness Vickers test was also carried out using 200 g load and 15 s period of loading. All the above tests were carried out at 300 K.

2.5. Sliding wear tests

Wear resistance tests, were carried out using pin-on-ring machine, under dry sliding conditions in ambient air at 300 K. The specimen was a cylindrical pin of 8 mm diameter and 12 mm height. Hardened steel ring (with HV 8100 MPa) of 70 mm diameter and 10 mm thickness was used as a counter body. During the tests the pin was pressed against the ring with variable loads of 180, 265 and 445 N. Three sliding speeds were chosen being 0.57, 0.95 and 1.53 m/s. Five sliding distances were selected, starting from 0.5 km with interval of 1–4.5 km. Three tests were performed for each set of condition and the average was taken.

3. Results and discussion

3.1. Metallography

Fig. 2 shows the as polished structures (a, b, and c) and matrix constituents (d, e, and f) for the 3 types of DI. Table II shows the nodule characteristics and volume fraction (V_f) of matrix constituents for the 3 types. The nodule count of conventional DI and ADI are the same but differ from that of low alloyed DI, this difference may stem from different chemical compositions among the irons [4]. This directly leads to the variation in the nodule size. The present results are in good agreement with Fatahalla, *et al.* [6], in which they showed that nodule size is inversely proportional to nodule count of DI. Comparing the %nodularity of conventional DI and ADI, Fig. 2a and b, it can be seen that there is no change in the nodule characteristics. The present results are in good agreement with Rao and Putatunda [7] in which they stated that the number of graphite patches, their size, distribution and nodularity are unaffected by austempering treatments and are influenced only by melting and casting practices. Fig. 2d reveals, graphite nodules embedded in a ferritic–pearlitic matrix, known as bull's-eye structure (cf., arrow in photo (d)). Fig. 2e shows that the matrix of ADI generally consists of upper bainite (B) (acicular) and retained austenite (non-transformed white regions (cf., arrow in photo (e)). No evidence of intercellular martensite or austenite decomposition products (carbides) was seen in ADI. This structure agree with results of Korichi, *et al.* [8] in which they indicated that during austempering at 713 K after austenitising at 1173 K the austenite transformed first to upper bainite that was coarser than that obtained at 653 K. Fig. 2f shows the graphite nodules surrounded by ferrite (F), pearlite (P), and iron carbides occurring in the internodular regions (cf., arrow

TABLE II Nodule characteristics and volume fraction (V_f) of matrix constituents for 3 types of DI

Alloy type	Nodule characteristics			Constituent phases volume fraction (%)					
	Nodule count	Nodule size (μm)	% Nodularity	Graphite	Ferrite	Pearlite	Retained Austenite	Upper Bainite	Iron Carbide
Conventional	90	45	95	20	50	30	—	—	—
ADI	90	45	95	20	—	—	20	60	—
Low alloyed	65	70	94	15	25	40	—	—	20

$$\% \text{ Nodularity} = \frac{\text{Number of graphite nodules}}{\text{Total number of graphite particles}} \times 100$$

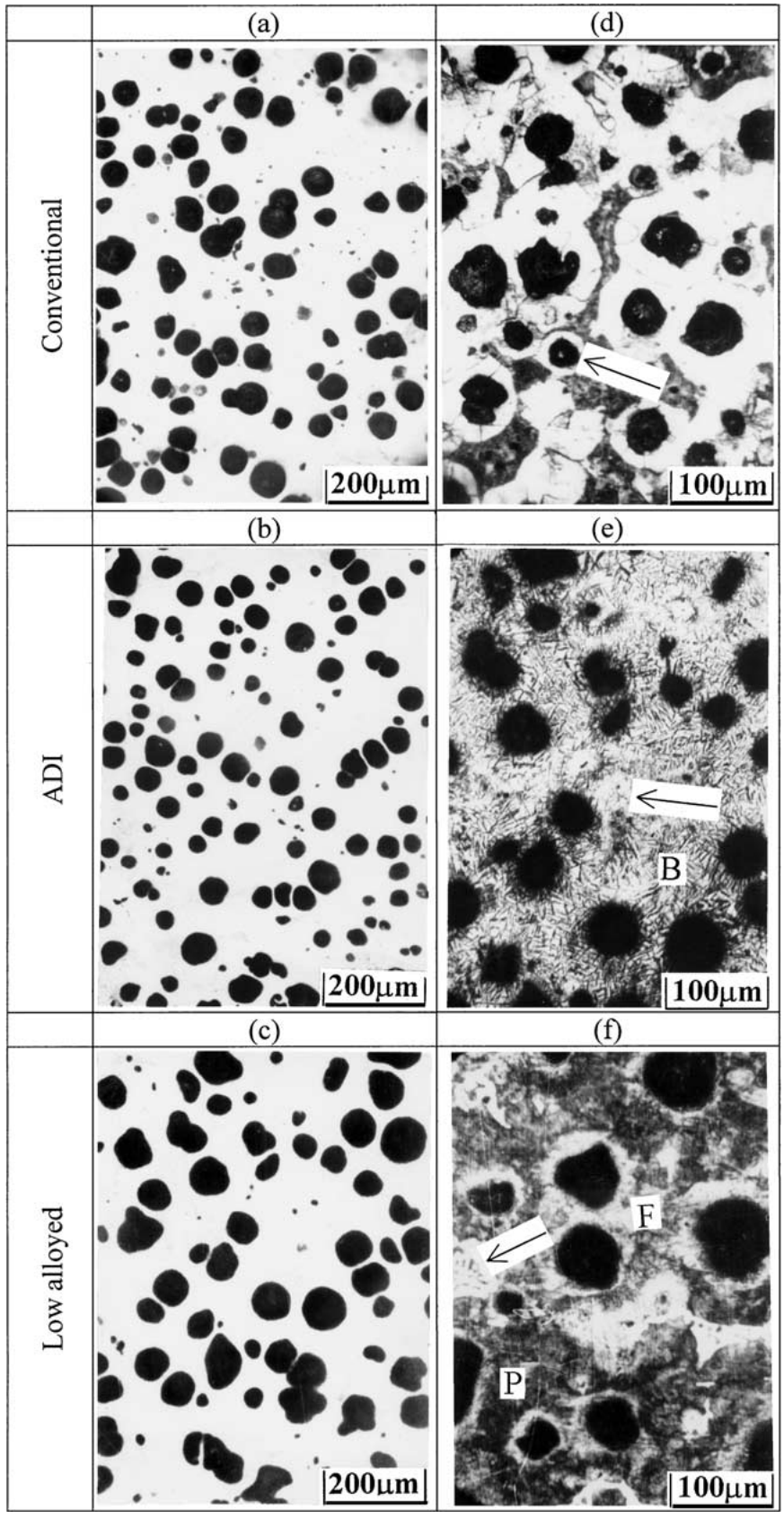

Figure 2 Nodule and matrices characteristics for the 3 types investigated of DI as revealed by optical microscope for as polished specimens (A, B, and C) and after etching with nital 2% (d, e, and f).

in photo (f)). This structure confirms that obtained by Muthukumarasamy [2] who indicated that the low alloy addition leads to the formation of intercellular carbides. Moreover, he indicated that repetition of production of bainitic DI in the as-cast condition based on Ni and Mo can be achieved. It can be seen in Table II that, the V_f of ferrite has a higher value than that of pearlite in the matrix of conventional DI. This may refer to the chemical composition of the matrix and high carbon equivalent [9]. Doubrava [10] concluded that the

chemical composition of the iron has been established as one of the significant factors determining the matrix structure. Silicon and carbon are expected to favour ferrite over pearlite. The V_f of upper bainite has a higher value than that of retained austenite in the matrix of ADI. This refers to the higher austempering temperature, which leads to faster rate of carbon diffusion and consequently, the growth rate of these ferritic platelets is rather rapid. Putatunda, *et al*. [11] concluded that the V_f of retained austenite in the matrix increases with increasing the austempering temperature, whereas the V_f of ferrite decreases as the austempering temperature increases. The V_f of pearlite has a higher value than that of ferrite, and iron carbide in the low alloyed DI matrix. This may refer to presence of elements such Ni, Mo and Cr that favour formation of pearlite and carbides. It can be noted from Table II that, the V_f of graphite in low alloyed DI showed lower values than that of conventional DI and ADI. Although the theoretical determination of the V_f of graphite in such DI results in a value around 12% [12]. However, Table II revealed higher values for all types investigated. This phenomenon is believed to refer the high SCR on the industrial scale which in turn results in the movement of the eutectic point to the higher carbon side and additionally to the chemical composition of the alloy [12].

3.2. Tensile properties

Fig. 3 shows the stress versus plastic strain diagram of the 3 types of DI. Using load-elongation curve, the values of tensile properties for the 3 types of DI were determined and listed in Table III. It shows that, the conventional DI has highest ductility ($\varepsilon_{max} = 14\%$) and toughness (49 MPa) than those of other two types. While the low alloyed DI shows higher tensile strengths ($\sigma_{pr(0.2)} = 750$ MPa and $\sigma_u = 1020$ MPa). This may be attributed to the presence of iron-carbide in the structure of low alloyed DI, which leads to increase of strength. The present results agree with Cox [13] who recorded σ_u for low alloyed DI (2.3% Ni, 0.76% Mo and 0.4% Mn) ranging from 850–1000 MPa. The results of tensile properties of ADI showed a bit lower values if compared with literature [14]. This can be attributed to the higher austempering temperature (723 K), which leads to coarser structure. However, the austempering temperature used in the literature was 648 K [14]. The present results agree with Jeng [15] who concluded that, at higher austempering temperatures, more stable retained austenite is created and then the tensile strength decreases. The results of conventional DI showed a bit higher values if compared with literature, which shows (in grade 65-45-12 of ASTM A 536) $\sigma_u = 448$ MPa and ductility of 12%. The slight difference is due to different SCR, which in turn affects of the internal stresses after casting [12]. It is well known that for ductile iron the matrix constituents and their volume fractions mainly control the tensile properties [14]. The %elongation of conventional DI shows a bit higher value (14%) if compared with grade 65-45-12 of ASTM A 536 in the literature [14]. It shows %elongation of 12%. This is believed to stem from the higher percentage of V_f of the softer phase (ferrite). The %elongation of ADI showed a bit lower value (6%) if compared with Grade 1050-700-7 of ASTM A 897: 1990, [14]. The latter showed %elongation of ADI of 7%. This comparison between the present investigation with the above two grades is done since they reveal the nearest properties with the present results. Bayati and Elliott [16] reported that, σ_u values show a decreasing trend with increasing austempering temperature, while the elongation values show an increasing trend up to 673 K, and, thereafter, decreases. The decrease in elongation values above 673 K is attributed to the change in the morphology of bainite (from a stronger lower bainite to a relatively weaker upper bainite). %elongation of the low alloyed DI showed lower values if compared with the other two types. This stems from the increase of tensile strength and hardness, which is a concomitant result of presence of alloying elements. The present results agree with Cox [13] who recorded that the elongation of low alloyed DI (2.3%

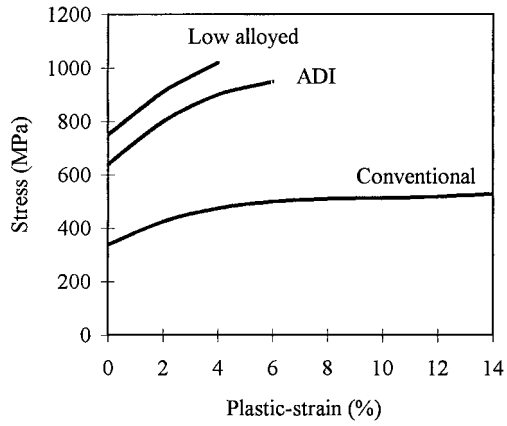

Figure 3 Stress versus plastic strain diagram of the 3 types of DI.

TABLE III Tensile and impact properties of the 3 types of DI for V-notched and unnotched specimens

	Tensile properties				Impact properties				
					V-notched		Unnotched		
Alloy type	σ_{pr} (0.2%) (MPa)	σu (MPa)	ε_{max} (%)	Toughness[a] (MPa)	Energy absorbed (J)	Impact strength (J/cm^2)	Energy absorbed (J)	Impact strength (J/cm^2)	Notch sensitivity factor
Conventional	340	528	14	49	17	26.56	110	110	0.24
ADI	640	950	6	38	5.6	8.75	60	60	0.146
Low alloyed	750	1020	4	27	2.8	4.37	5	5	0.874

[a]Toughness values in this table were detected from the tensile stress strain diagram.

The values in this table were detected from the impact test, taking into consideration the specimen's dimensions are: (volume = 5500 mm^3).

Notch sensitivity factor $= \dfrac{\text{Notched strength}}{\text{Unnotched strength}}$. (See reference 21).

Ni, 0.76% Mo and 0.4% Mn) ranged from 3.5–5%. As shown in Table III the toughness results of conventional DI shows the highest value if compared with the other two types. The increase of toughness is in consistence with the increase of ductility. Kobayashi and Yamada [17] concluded that, the increase of toughness is caused mainly by the increase in ductility. The toughness of conventional DI is about 1.3 times that obtained in ADI and about 1.8 times that obtained in low alloyed DI. This good toughness of conventional DI is due to the fact that, when the V_f of ferrite phase increases the toughness also increases and reaches a peak value when V_f of ferrite is around 60% [18]. The lower toughness of ADI than conventional DI results from the high transformation temperatures up to 723 K. Johansson, [19] concluded that when the transformation temperatures exceeds 673 K, the toughness substantially decreases. The lower toughness of low alloyed DI than both two types is related to the fact that this material contains iron carbides due to alloying elements. These carbides are known to reduce the toughness [11]. Table III shows that the toughness of ADI (38 MPa) is higher than that of low alloyed DI (27 MPa), which indicates that the addition of alloying elements like nickel and molybdenum is not recommended as far as the toughness is concerned.

3.3. Impact properties

Table III shows also the values of impact property of the 3 types of DI. The highest values of energy absorbed and impact strength for both tests were observed for conventional DI. This refers to the increase in %elongation of conventional DI, if compared with other two-type [20]. Fig. 4 shows a histogram comparing among the impact strength and ductility (%elongation) for the 3 types of DI. It can generally, be seen that the impact strength increases with increasing ductility. Table III shows also that, the notch sensitivity of ADI is higher than those of conventional DI and low alloyed DI. On the other hand, the %elongation of ADI is intermediate between the other two types. This discrepancy in the trend of notch sensitivity and ductility maybe justified by Young [21] who indicated that, there seems to be no direct correlation between the notch sensitivity and ductility. Notch sensitivity correlate with other mechanical properties, e.g., the shape of stress–strain diagram, the damping properties, the modulus of elasticity and the work hardening properties [21]. The energy absorbed and the impact strength of ADI are intermediate between the other two types. The impact energy of ADI showed a bit lower value if compared with literature [14]. This result agree with Muthukumarasamy, *et al.* [2] in which they concluded that, the impact energy showed an increasing trend corresponding to austempering temperature of 623 K after which there is a considerable decrease. Grech, and Young [22] reported that the impact energy values of unnotched specimens reached a maximum at a temperature of 623 K and fell with further increase in austempering temperature. The low alloyed DI shows the lowest value of impact energy due to the presence the of Ni, Mo and Mn. The present results of low alloyed DI agree with [2] in which they recorded that the impact energy values of as-cast DI alloyed with 2.4% Ni and 0.05% Mo is 2.5 J. Aoyama and Kobayashi [23] concluded that the absorbed energy was found to be markedly decreased as the Ni content was increased.

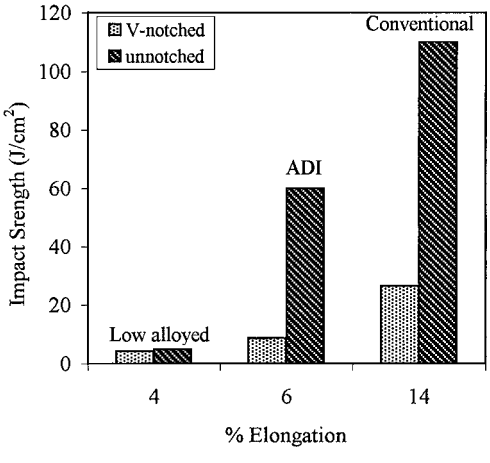

Figure 4 Histogram illustrating a comparison among the impact strength and ductility (%elongation) for the 3 types of DI.

3.4. Fracture surface observations

Figs 5a and b shows the features of the fracture surface of the conventional DI as observed after failure in a tensile and impact tests. Fig. 5a shows ductile mode of fracture characterised by smooth ripple pattern (marked R). This can be detected from the relatively large cavity-size in comparison with the graphite nodule size. Fig. 5b reveals ductile fracture characterised by dimple pattern around the graphite nodules (marked D). Comparing between Fig. 5a and b we can observe that the clearances between the graphite nodules and their corresponding cavities are observed to be larger in tensile test than that of impact test as indicated by arrows. This is believed to be due to the plastic deformation, which occurred during simple tension at relatively low strain rate [22]. The reason of the presence of ripple pattern in tensile test specimens and dimple patterns in impact test specimens, is due to the reduction of the triaxility ratio in the matrix as a result of superposition of hydrostatic pressure during tension [22]. Figs 5c and d show the features of the fracture surface of the ADI as observed after failure in tensile and impact tests. The main feature of Fig. 5c is dimple pattern (D) with small quasi-cleavage areas as indicated by (Q). While the main feature of Fig. 5d is a quasi-cleavage (Q) fracture with some fine dimple areas (D). In comparison with the results obtained for conventional DI, for both tests, we notice that, the clearances between the graphite nodules and their corresponding cavities are observed to be tighter as indicated by arrows in Figs 5c and d if compared with Figs 5a and b. It is to be pointed out that, the fracture mode in the impact test reveals little deformation with no stretching around the graphite nodules [24]. Taha and Fatahalla [25] presented a model to measure the clearance between the graphite nodules and their corresponding cavities from fracture surface observations.

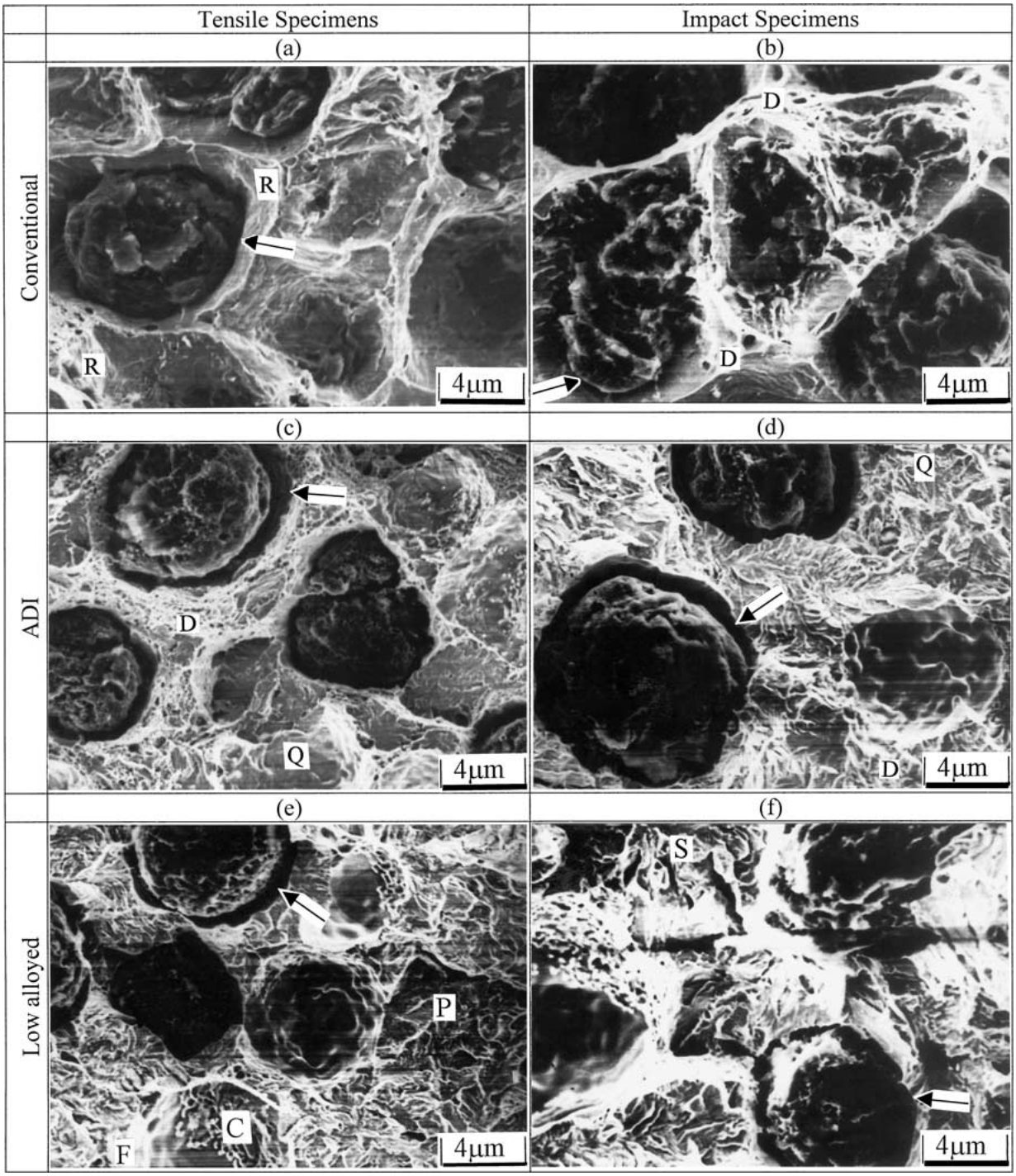

Figure 5 Fracture surface features as revealed by SEM of the 3 types of DI ruptured under tensile and impact loading.

Thereafter, a correlation between this model and ductility of DI was also presented. Additionally a model was proposed for secondary carbon precipitation on the graphite nodules and its probable effect on the ductility of the ingot. The results of the present investigation is in good agreement with Aranzabal *et al*., [26] in which they concluded that, for specimen austempered at 683 K (high temperature) the microstructure corresponds to an upper bainite with high quantities of austenite (>30%). In this situation the fracture mechanism is quasi-cleavage. Figs 5e and f show the features of the fracture surface of the low alloyed DI as observed by SEM after failure in tensile and impact tests. Fig. 5e shows the ferrite areas (F) are small if compared to the pearlite (P) and carbide areas (C). This structure indicates the lack of plastic deformation occurring in the matrix. In comparison with the results obtained for ADI, the cavity contour can be seen to bound the graphite nodules with small clearances as indicated by arrow in Fig. 5e if compared with Fig. 5c. This small clearance indicates slight occurrence of plastic deformation around the graphite nodules. While Fig. 5f shows brittle mode with cleavage facets marked S. The cleavage facets plateau which indicate the brittle behaviour of fracture were observed to be of miniature size and a little bit different in nature. In comparison with the results obtained for ADI, the clearance between the graphite nodules and their corresponding cavities are

observed to be tighter as indicated by arrow in Fig. 5f if compared with Fig. 5d. This appearance leads to the lack of plastic deformation occurring in the matrix. The cleavage fracture surface, observed in the low alloyed DI, was due to the presence of iron carbides formed in the matrix. That is; the reason for marked loss in toughness of low alloyed DI. The present results are consistent with Aoyama and Kobayashi [23] in which they concluded that the marked loss of toughness, revealed the cleavage fracture on the part of embrittled impact specimen. Bartosiewicz *et al*. [18] concluded that, the presence of Cr added to the iron leads to reduction of toughness because it produced segregation. The elements, such as Si and Mn, lead to excessive interdentritic segregation and they help carbides to form. This carbide precipitates in the intercellular regions and results in brittle fracture, which causes the reduction in toughness.

3.5. Hardness

Table IV shows the hardness values for the 3 types of DI. The lowest values refer to conventional DI. The present hardness values resembles the ASTM A 536 of DI, grade 65-45-12 [14] which showed, the Brinell hardness (HB) values ranging from 1400–1800 MPa. ADI revealed intermediate hardness values which may stem from an increase in austempering temperature (723 K) which leads to a reduction in strength and hardness if compared with low austempering temperature (573 K), which have a HV value of 5300 MPa. Stenfors *et al*. [27] concluded that, the hardness decreased when the austempering temperature is increased and a minimum is observed at about 673 K. The hardness results of the present ADI resemble those of grade 1050-700-7, of ASTM A 897: 1990, [14] which shows the HB values ranging from 3020–3630 MPa. Table IV shows that, the highest hardness values refers to the low alloyed DI, which is believed to be due to the presence of alloying elements (Ni, Mo and Cr) which in turn cause the formation of harder phases such as carbide and pearlite as shown in the microstructure given in Fig. 3c. Muthukumarasamy, *et al*. [2] recorded the macrohardness of as-cast DI alloyed with 2.4% Ni and 0.05% Mo is Rc 33 (tempering at 873 K for 7.2 ks). They indicated also the hardness value of ADI alloyed with 2% Ni as HB 4200 MPa. The present results show higher values compared with Muthukumarasamy *et al*. [2]. The discrepancy may stem from the following:

1. Muthukumarasamy, *et al*. [2] used a Mo content at 0.05%, while in the present research, the Mo content was 0.52%.

2. Muthukumarasamy, *et al*. [2] did not use Cr or Mn, while it is 0.75%Cr and is 0.6%Mn in the present research.

The Vickers microhardness results of ferrite and pearlite (matrix constituents) of conventional DI agree with many investigations. Skaland [28] reported the microhardness of ferrite and pearlite to be approximately HV 1700 and 2900 MPa respectively. Angus [29] reported that the hardness of ductile iron varies according to its matrix type and composition. With a fully ferritic matrix, values of HV ranging from 1500–1800 MPa respectively, and for a pearlitic matrix HV values ranging from 2500–3000 MPa respectively. Avner [30] reported the pearlite HV ranging from 2230–3020 MPa. The microhardness HV value of bainitic constituent of ADI shows 3730 MPa. This value agrees well with Janowak [31] who stated that the HV of bainite ranging from 3000–5000 MPa. The bainitic constituents showed higher value when compared with the grade (1050-700-7) of ASTM standard A 897 M:1990. It shows the HB of the bainite ranging from 3020–3630 MPa. This maybe due to the variations in chemical compositions and increase in the volume fraction of the harder phase (upper bainite) compared with retained austenite. It may also refer to the different procedures used in the two researches, and additionally, due to the complexity of defining the hardness property and the factors that affects it [6]. The retained austenite of ADI, showed a consistent value with Janowak [31] who stated that the HV of austenite ranging from 1000–4000 MPa. The ferrite, pearlite and iron carbides of low alloyed DI showed a consistent value with Janowak [31], who stated that the HV of ferrite, pearlite and iron carbide ranging from 1000–2500 MPa, 1750–4000 MPa, and 10000–20000 MPa respectively. Angus [29] reported the HV of carbide in DI ranging from 6000–10000 MPa.

4. Wear characteristics

4.1. Variations of mass loss versus sliding distance at constant load

Fig. 6 shows the variation of mass loss versus sliding distance for the 3 types of DI at constant load (265 N) and constant speed (0.95 m/s). The wear characteristics for the 3 types follow the normal wear behaviour of metals and alloys [3]. In other words, the low alloyed DI showed that the running-in period start from zero to 4.5 km. The running-in period of ADI starts from zero and continues up to 1.5 km of sliding distance. After 1.5 km of sliding the mass loss monotonically increased up to 2.5 km. After 2.5 km the mass loss seems

TABLE IV Hardness conversion table of the 3 types of DI

	Hardness									
			Rockwell			Vickers microhardness (MPa)				
Alloy type	HB (MPa)	HV (MPa)	A	B	C	Ferrite	Pearlite	Austenite	Upper Bainite	Carbide
Conventional	1820	1850	51	—	—	1650	2600	—	—	—
ADI	3180	3200	—	59	33	—	—	3300	3730	—
Low alloyed	4420	4600	—	61	45	2830	4000	—	—	6000

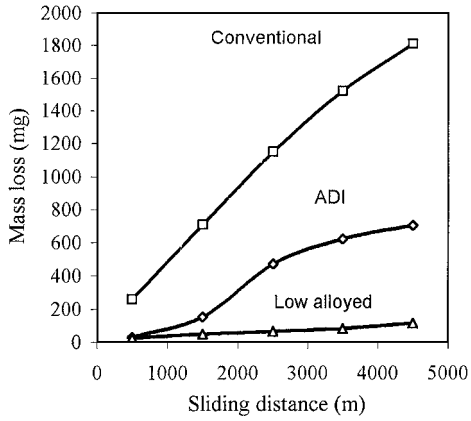

Figure 6 Relationship between mass loss and sliding distance for the 3 types of DI at constant load of 265 N and constant speed of 0.95 m/s.

to be steady until 4.5 km. Fig. 6 shows also that, the conventional DI reveals the highest mass loss (lowest wear resistance). On the other hand, the low alloyed DI shows the lowest mass loss, revealing the highest wear resistance. The ADI curve is intermediate between the other two curves, however it is much closer to the low alloyed DI than that of conventional DI, reflecting the relatively good wear resistance of the ADI material as compared to the low alloyed DI. The highest mass loss of conventional DI refers to its relatively low hardness. The intermediate values of mass loss of ADI are related to the intermediate hardness values. It may also related to the amount of retained austenite. The increase in austenitising and austempering temperatures decrease the bulk hardness because of the increased amount of retained austenite, resulting in an increase in mass loss of ADI greater than that of low alloyed DI. This result agrees with Jeng [15] who concluded that the wear resistance absolutely depends on the amount of retained austenite and the hardness of the matrix structure. The low alloyed DI showed superior wear resistance compared to the other two types, this may refer to the high hardness which is a good indication of the low mass loss. The main reason for the low mass loss of harder specimens is the low plastic deformation adjacent to the graphite particles [32]. The mass loss is directly related to hardness [32]. The hardness versus mass loss for the 3-types of DI is illustrated in Fig. 7.

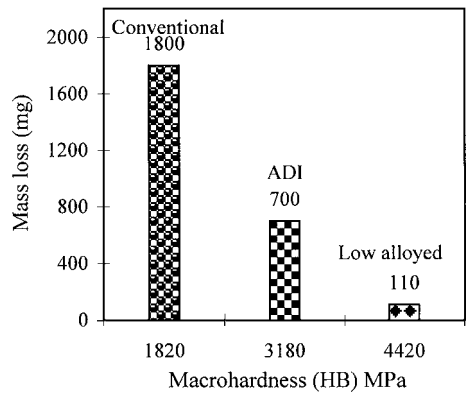

Figure 7 Histogram illustrating a comparison of mass loss, at 4500 m sliding distance, versus Brinell hardness for the 3 types of DI.

4.2. Variations of mass loss with sliding distance at different loads

Fig. 8a and b illustrate the variation of mass loss with sliding distance at different loads for low alloyed DI and ADI respectively. As shown in the two figures, the effect of increasing the load and sliding distance is to increase the mass loss. Fig. 8a reveals that, at low and medium loads (180 N and 265 N) the mass loss shows approximately linear relationship with sliding distance with no indication of an initial transient stage of mild to severe wear from beginning to end of the curves. This phenomenon refers to the surface of the pin, specimen in the wear test, which was relatively smooth with only minor surface grooves. For relatively high load (445 N) of testing, after 2.5 km of sliding distance there is a drastic increase (severe wear) up to 4.5 km. This phenomenon refers to the surface of the pin which is irregular and heavily damaged giving further indication that a basic change in wear behaviour has occurred. These features are characteristic of a mild-to-severe wear transition. Fig. 8b shows that at low load (180 N) the mass loss was relatively small and it shows almost linear relationship from beginning to end of the curve. For medium load (265 N) the running-in period starts from zero and continued up to 1.5 km of sliding distance. After 1.5 km the mass loss monotonically increased up to 2.5 km. increased up to 2.5 km. After 2.5 km the mass loss seems to be steady until 4.5 km. For high load (445 N), the mass loss increased remarkably from beginning to end of the curve. It is also noted that there is no indication of transition period and most of the curves revealed severe wear. At low loads the mild wear was observed for a wide range of sliding distances in the ADI. On the other hand, its range in the low alloyed DI was very narrow. The low values of mass loss of low alloyed DI is due to presence of alloying elements such as molybdenum, which is mild carbide former. Angus [29] concluded that, adding molybdenum at levels of 0.5% or more, results in appearance of some grain boundary carbides. This carbide stabilising effect will be accentuated by the presence of other carbide-stabilising element, such as Cr, Mn, and V. The structure of the matrix, as well as the hardness and wear resistance is markedly affected by the presence of carbides [32].

4.3. Variation of mass loss with sliding distance at different speeds

Fig. 9a and b show the variation of mass loss with sliding distance at different speeds of low alloyed DI and ADI respectively. As is shown in the two figures, the effect of increasing the sliding speed is to increase the mass loss. Fig. 9a shows that, at low and medium speeds (0.57 m/s, 0.95 m/s) the mass loss is somewhat regular with low values (mild wear), and monotonically increased until 4.5 km. For a relatively high speed (1.53 m/s) the curve showed normal behaviour up to 2.5 km of sliding distance. Thereafter, a drastic linear increase (severe wear) is observed up to 4.5 km. Fig. 9b shows that, at low speed (0.57 m/s) the mass loss was relatively small and it shows linear relationship from beginning to end of the curve. At medium speed

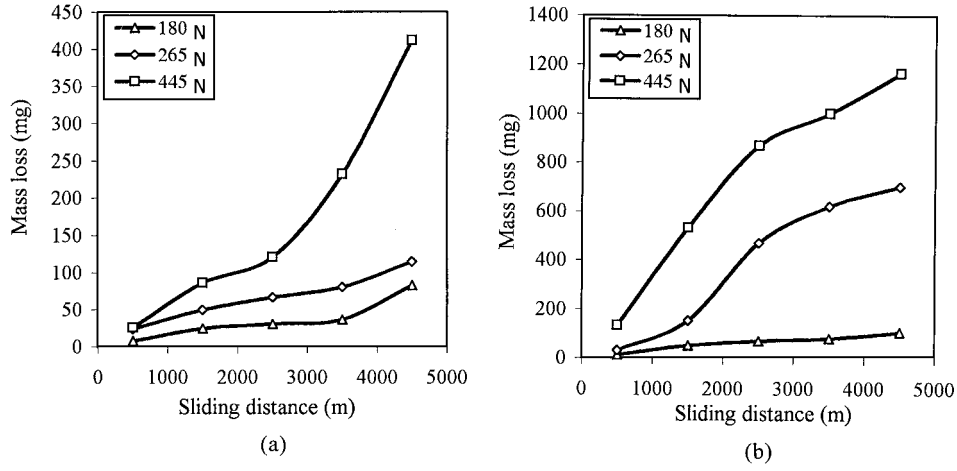

Figure 8 Relationship between mass loss and sliding distance at different loads and constant speed (0.95 m/s) of low alloyed DI and ADI.

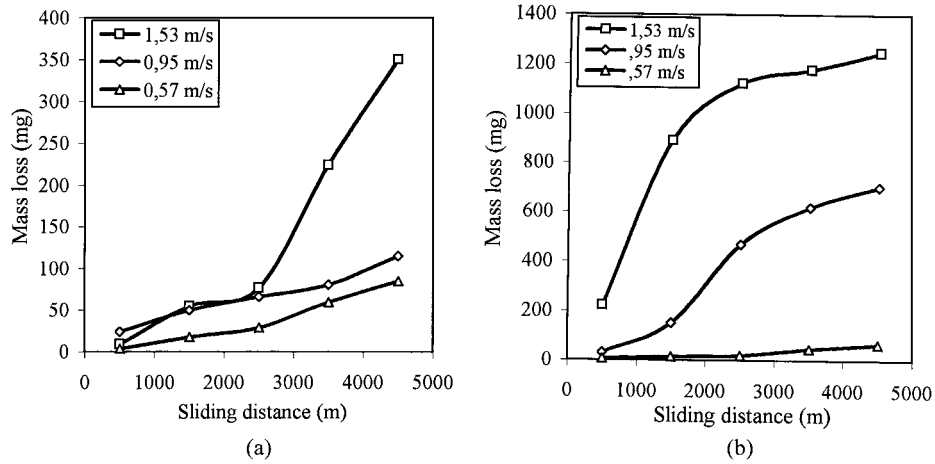

Figure 9 Relationship between mass loss and sliding distance at different speeds and constant load (265 N) of low alloyed DI and ADI.

(0.95 m/s) the running-in region starts from zero to 1.5 km of sliding distance. Thereafter, a monotonic linear increase is observed up to 4.5 km. At relatively high speed (1.53 m/s) the mass loss is increased drastically up to 1.5 km of sliding distance. Thereafter, monotonic gradual increase occurred up to 2.5 km. After 2.5 km the mass loss seems to be steady until the end of the curve. The increase in mass loss at higher speeds can be attributed to more irregular surfaces. The increase of sliding speed make the rubbing surface rough due to wear particles interferes from pin entrapped between the two rubbing surfaces. It may also be due to the high temperature and vibration generated during the test at high speeds. Terheci, *et al.* [33] concluded that the increase in mass loss observed at higher speed is a result of vibrations which in turn are mainly the result of higher impact shocks exerted by the two rubbing surfaces, one against another. They also concluded [33] that the amplitude of these vibrations increased with increasing speed and particle size. The amount of particles generated depends mainly on number of cycles (time) and load (depth of plastically deformed zone). This confirms the present results, where at high load and speed the mass loss is increased drastically (severe wear). On the other hand, at low load and speed the mass loss did not change considerably (mild wear).

4.4. Variation of coefficient of friction with sliding distance at constant and different loads

Fig. 10 shows the coefficient of friction (μ) versus sliding distance at constant load and speed for the 3 types of DI. It can be seen that the highest values of coefficient of friction refer to the conventional DI and the lowest refers to the low alloyed DI. On the other hand, the values of coefficient of friction of ADI are intermediate

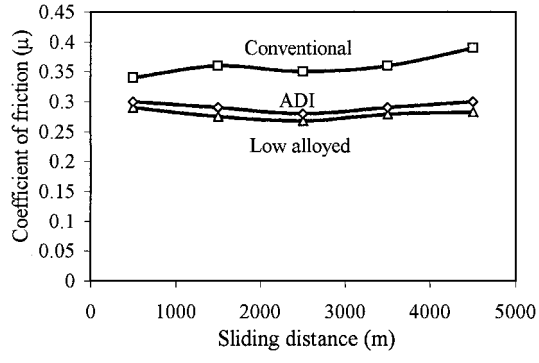

Figure 10 Relationship between coefficient of friction (μ) and sliding distance for the 3 types of DI at constant load (265 N) and speed (0.95 m/s.)

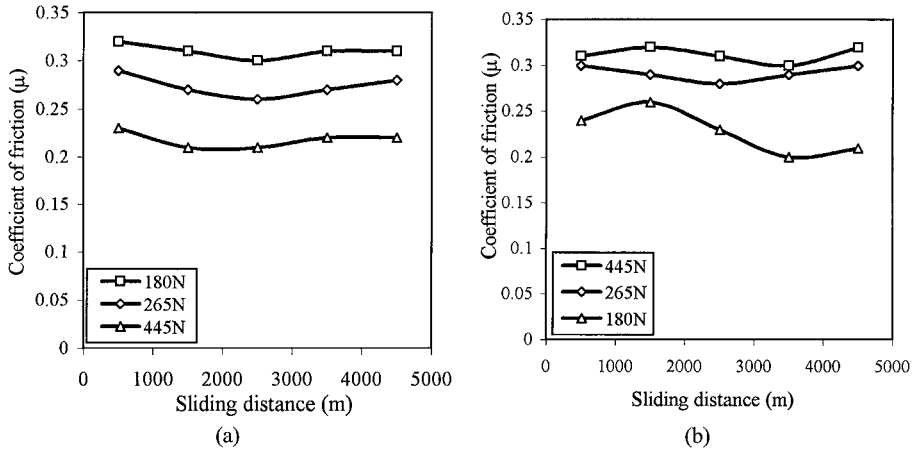

Figure 11 Relationship between coefficient of friction and sliding distance at different loads and constant speed (0.95 m/s for the low alloyed DI and ADI.

between the other two types. Fig. 11a reveals the coefficient of friction versus sliding distance for low alloyed DI at different loads and constant speed of 0.95 m/s. It can be seen that the coefficient of friction is highest for the lowest load and vice versa. Fig. 11b reveals the coefficient of friction versus sliding distance for ADI at different loads and constant speed of 0.95 m/s. It can be seen that the coefficient of friction is highest for the highest load (445 N) and it is lowest for the lowest load (180 N). The coefficient of friction for conventional DI is high because of the tendency to adhesion of soft ferrite matrix. The lower coefficient of friction of low alloyed DI and ADI than that of conventional DI is believed to be due to the difficulty of adhesion of the hard carbide matrix in low alloyed DI and bainite matrix in the ADI. The present results are in a good agreement with Islam, *et al*. [34] in which they observed that the friction response is affected more by the surface hardness while the wear response is essentially controlled by the material microstructure [34]. The coefficient of friction fluctuates by a large amount with the higher value being governed by the deformation and strength of adhesive bonds and the lower value resulting from their rupture. As a result of this, the sliding is not smooth and it indicates that the graphite film, which formed on the sliding surface due to the presence of graphite in DI, is not effective in suppressing the adhesive bonding at the sliding interface. In pin-on-ring contact, high stresses develop at beginning of the test. As the pin and ring starts wear, the actual contact stresses reduce and the contact area enlarges. The stresses remain however significantly higher than the nominal stresses under a flat pin sliding on ring.

4.5. Study of wear track

Fig. 12a, b and c shows optical micrographs of longitudinal sections perpendicular to the worn surface (indicated by arrow) of specimens tested through wear of conventional DI, ADI and low alloyed DI respectively. It can be seen that the edges of conventional DI sample is irregular and much more corrugated, as in Fig. 12a

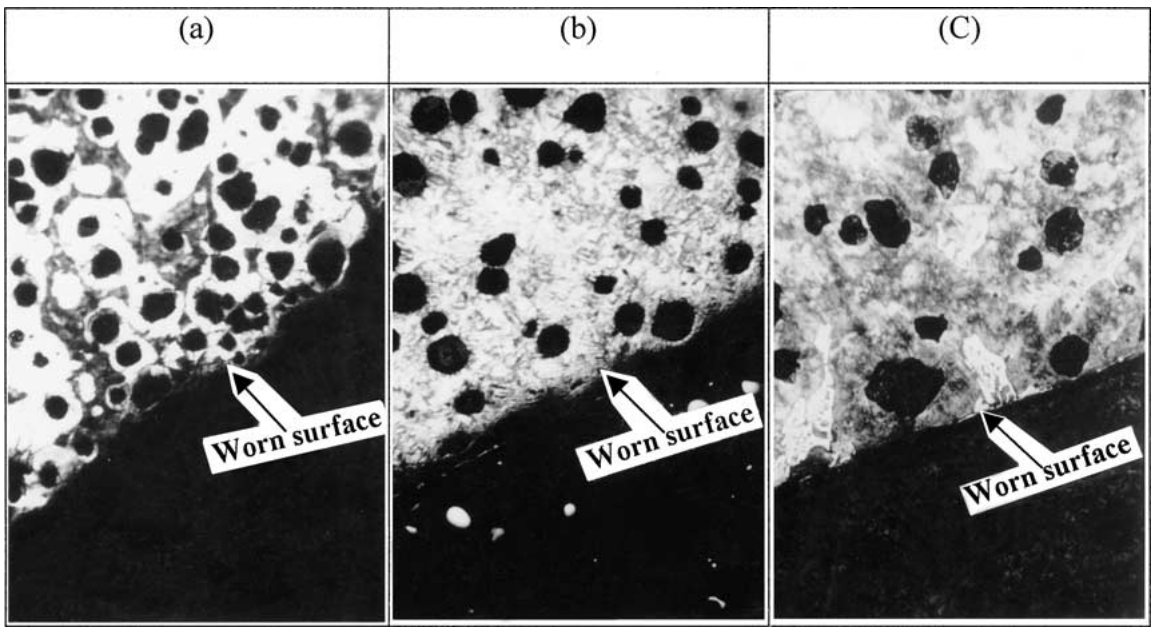

Figure 12 Optical micrographs showing longitudinal cross sections near the worn surfaces of (a) conventional DI, (b) ADI and (c) low alloyed DI.

while the edge of ADI is a little bit corrugated as in Fig. 12b. The edge of low alloyed DI sample is slant as in Fig. 12c. The worn surfaces of the 3 types show that, the mode of particle deformation is mainly by surface adhesion and plastic deformation. The present results of wear characteristics are strongly related to the microstructure of the 3 types of DI, which indicated that the low alloyed DI is higher wear resistance than that of conventional DI and ADI. This is clearly demonstrated by the lower plastic strain (slant edge) of low alloyed DI than those of the other two types (corrugated edges). When the load is applied, the three samples exhibit what appears to be work hardened layer. This layer developed increased in thickness with increasing load on the surface in the mild region. Increasing the load seems to increase the surface temperature, further metallographic examination and hardness testing indicated that, this layer was essentially carbide in the low alloyed DI samples. Zhou, *et al*. [35] presented a section of a specimen austempered at 573 K with high hardness (Rc 38), the structure consisted of lower bainite and less retained austenite. They observed that the worn surface was quite smooth and has a better wear condition. The structure of the section of specimens austempered at high temperatures 673 K with a low hardness (Rc 20), consisted of upper bainite and more retained austenite. They observed that its wear rate was high and the worn surface was quite rough. These previous results agree with the present investigation in which the harder specimens showed slant edge and the softer shows corrugated edge.

4.6. Subsurface microhardness investigation

Fig. 13 shows the microhardness testing results of the 3 types of DI. It is generally, noted that the microhardness near the worn surface is much higher than that in the bulk, however in the case of conventional DI the variation of hardness has much wider thickness than ADI and low alloyed DI. If we compare the ADI with low alloyed DI we find also that the deformed layer in ADI is much wider than in the low alloyed DI. Measurements showed that, the thickness of the hardened layer of conventional DI, ADI and low alloyed DI were 260 μm, 200 μm, and 160 μm respectively. The bulk hardness increased from 6000–7800 MPa near the worn surface of the low alloyed DI. Additionally, from 3300–4800 MPa for ADI, and from 1650–3000 MPa for conventional DI. This increase is due to the subsurface deformation produced in sliding under a load of 265 N. Generally speaking, the microhardness values are decreasing with increasing the distance from the worn surface and thereafter, it becomes steady state. The increase in hardness near the worn surface during wear is reported by others [3, 36]. Islam, *et al*. [34] concluded that the increase in hardness of the as-cast samples is due to strain hardening of the matrix at the surface region which predominates over any frictional heating effect. The worn surfaces in Fig. 12a, b, and c are strongly related to the microhardness curves given in Fig. 16. The deformed layer of conventional DI is wider than that of other two types. This is due to its lower hardness than those of ADI and low alloyed DI. The higher hardness reflects that the matrix is strengthened and can resist wear quite effectively. Sixton and Fischer [37] have found that the wear mechanism in steel depends upon its hardness. In martensitic steel with higher hardness, abrasive wear tends to take place. But for low hardness values, adhesive wear is encountered [38]. These results are in consistence with the present study. For low alloyed DI abrasive wear was found to be the main mechanism while for the softer conventional DI, adhesive wear took place. The present results are also in good agreement with a recent research [38] which presented the wear characteristics of austempered chilled ductile iron containing 0.1% Mo and Ni contents varying from 0.5 to 2.5%. It was found that wear resistance is highly dependent on the Mo and Ni content. Moreover, wear resistance also increases monotonically with hardness, tensile strength, and nodule count.

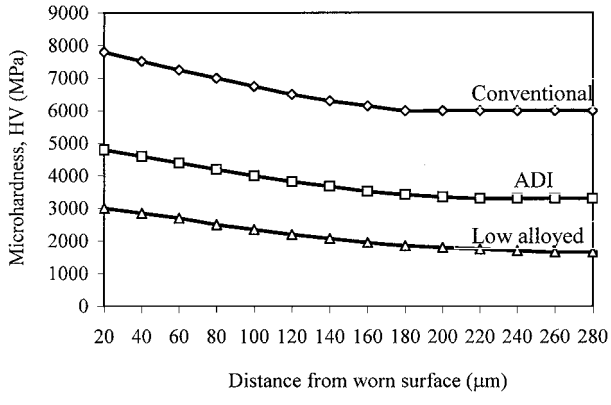

Figure 13 Variation of microhardness with distance from worn surface for the 3 types of DI under a load of 265 N and speed of 0.95 m/s.

5. Conclusion

1. ADI was successfully produced in the present investigation having properties comparable to those of low alloyed DI.

2. The impact strength of conventional DI was found to be 3 times that of ADI and 6 times that of low alloyed DI, for the V-notched specimens. On the other hand, for the unnotched specimens, conventional DI impact strength was found to be 1.8 times that of ADI and 22 times that of low alloyed DI. The impact strength was found to be directly proportional to ductility. No direct correlation between the notch sensitivity and ductility was found in the case of ADI.

3. The fracture modes of impact loading specimens of low alloyed DI and ADI revealed slight plastic deformation around the graphite nodules and the matrix failed in a brittle manner, as evidenced by the numerous cleavage and quasi-cleavage patterns. However, the fracture mode of conventional DI is ductile as evidenced by the presence of ripple and dimple patterns. The fracture surface of the specimens which failed under tensile testing revealed patterns reflecting more ductility than those failed under impact testing.

4. Hardness values of low alloyed DI was found to be 1.5 times greater than those of ADI and 2.5 times greater for conventional DI.

5. The mass loss of ADI was observed to be intermediate between the other two types, much closer to the low alloyed DI, reflecting relatively good wear resistance of the ADI material compared to the low alloyed DI.

6. Wear resistance was found to be mainly related to the hardness. The mass loss was found also directly related to the sliding speed and applied load. The coefficient of friction of conventional DI was found to be highest among those investigated.

7. The worn surfaces of conventional DI and ADI showed corrugated edges, while that of low alloyed DI showed slant edge. The microhardness near the worn surface was found to be higher than that in the bulk of the 3 types of DI, indicating plastic strain hardening occurred during the test.

Acknowledgements

The authors wish to express their gratitude to Prof. Saied Moustafa in the National Research Centre for support in studying the fracture surface using SEM. One of the authors (A. Refaey) wishes to express his gratitude to Prof. Adel Nofal, the Head of the Central Metallurgical Research and Development Institute (CMRDI) in Tebbin-Helwan-Egypt, for the support in studying the wear characteristics on the TNO-Tribometer machine. He also wishes to express his gratitude to Eng. Osama Hussein, the Manager of the Information Centre, El Nasr Company for Casings-Egypt, for kind supply of raw materials.

References

1. Cast Metals Development Ltd., Materials and Design **5** (1992) 285, (Butterworths-Heinemann Ltd.).
2. S. MUTHUKUMARASAMY, A. J. S. SABU and S. SESHAH, *Indian Foundry Journal* (1992) 23.
3. L. PING, BAHADUR and D. VERHOEVEN, *Wear* **138** (1990) 269.
4. N. FATAHALLA, S. BAHI and O. HUSSEIN, *J. Mater. Sci.* **31** (1996) 5765.
5. ASTM Designation: A 247-67 (Reapproved 1984) "Standard Method for Evaluating the Microstructure of Graphite in Iron Castings," Vol. 03.01 (Annual Book of ASTM Standards, 1996).
6. N. FATAHALLA, H. HAKIM, A. ABO ELEZZ and M. MOHAMED, *J. Mater. Sci*. **31** (1996) 4933.
7. P. PRASCO RAO and S. K. PUTATUNDA, *Metallurgical and Materials Trans*. **29A** (1998) 3005.
8. S. KORICHI and R. PRIESTNER, *Materials Science and Technology* **11** (1995) 901.
9. N. FATAHALLA, H. HAKIM and M. MOHAMED, *Z. Metallkd* **89**(7) (1998) 507.
10. J. H. DOUBRAVA, S. F. CARTER and J. F. WALLANCE, *AFS Trans*. **89** (1981) 229.
11. S. K. PUTATUNDA and I. SINGH, *Journal of Testing and Evaluation* **23** (1995) 325 [By the American Society for Testing and Materials].
12. N. FATAHALLA, T. GOMAA, S. BAHI and M. NEGM, *Z. Metallkd* **89**(8) (1998) 554.
13. G. J COX, *Foundry Trade Journal* **134** (1974) 741.
14. ASM, Metals Handbook, **1** (1993), 10th Edition, American Society For Metals, Metals Park, Ohio.
15. M. C. JENG, *J. Mater. Sci*. **28** (1993) 6555.
16. H. BAYATI and R. ELLIOTT, *Materials Science and Technology* **13** (1995) 319.
17. T. KOBAYASHI and S. YAMADA, *Metallurgical and Materials Transactions* **27A** (1996) 1961.
18. L. BARTOSIEWICZ, I. SINGH, F. A. ALBERTS, A. R. KRAUSE and S. K. PUTATUNDA, *Journal of Materials Engineering and Performance* **4** (1995) 90.
19. M. JOHANSSON, *AFS Trans. American Foundrymen's Society* **85** (1977) 117.
20. W. L. BRADLEY, in Proceedings of the International Conference on Mechanical Behaviour of Ductile Cast Iron and other Cast Metals, 30th July–1st August 1993, Kitakyushu, Japan, p. 42.
21. J. F. YOUNG, "Materials and processes" (1954) p. 117.
22. M. GRECH and J. M. YOUNG, *AFS Trans*. **98** (1990) 345.
23. M. AOYAMA and T. KOBAYASHI, in Proceedings of the International Conference on Mechanical Behaviour of Ductile Cast Iron and Other Cast Metals, 30th July–1st August 1993, Kitakyushu, Japan, p. 425.
24. H. Q. SU, M. YAN and X. L. GUO, in Proceedings of the International Conference on Mechanical Behaviour of Ductile Cast Iron and Other Cast Metals, 30th July–1st August 1993, Kitakyushu, Japan, p. 351.
25. T. GOMAA and N. FATAHALLA, in International Symposium on Designing, Proceeding and Properties of Advanced Engineering Materials, 1997, Toyohashi, Japan, ISPJ AEM 156 committee. 247.
26. J. ARANZABAL, I. GUTIERREZ, J. M. R. IBABE and J. J. URCOLA, *Materials Science and Technology* **10** (1994) 728.
27. S. E. STENFORS, J. STORESUN and R. SANDSTORM, in Proceedings of 2nd International Conference on ADI, Ann. Arbor, Michigan, USA, March 1986 (American Society of Mechanical Engineers) p. 227.
28. T. SKALAND, *Scandinavian Journal of Metallurgy* **21** (1992) 63.
29. H. ANGUS, "Cast Iron: Physical and Engineering Properties," 2nd ed. (Butterworths and Co., London, 1978).
30. S. AVNER, "Introduction to Physical Metallurgy," 2nd ed. (McGraw-Hill, Tokyo 1974).
31. J. F. JANOWAK, *Journal of Applied Metalworking* **4** (1986) 223.
32. Q. A. SHAIKH, *Materials Science and Technology* **7** (1991) 728.
33. M. TERHECI, R. R. MANORY and J. H. HENSLER, *Wear* **180** (1995) 78.
34. M. A. ISLAM, A. S. M. A. HASEEB and A. S. W. KURNY, *ibid*. **188** (1995) 65.
35. W. S. ZHOU, Q. ZHOU and S. K. MENG, *ibid*. **162–164** (1993) 696.
36. J. M. PRADO *et al*., *Materials Science and Technology* **11** (1995) 294.
37. M. D. SEXTON and T. E. FISCHER, *Wear* **96** (1984) 17.
38. J. HEMANTH, *Materials and Design* **21** (3) (2000) 139.

Received 16 July 2001
and accepted 8 July 2002